Front. Earth Sci. 2019, 13(3): 614–627
https://doi.org/10.1007/s11707-018-0747-3

RESEARCH ARTICLE

Spatiotemporal influences of land use/cover changes on the heat island effect in rapid urbanization area

Ying XIONG[1,2], Fen PENG[1,2], Bin ZOU (✉)[3]

1 Research Center of Resource Environment and Urban Planning, Changsha 410114, China
2 School of Architecture, Changsha University of Science & Technology, Changsha 410114, China
3 School of Geosciences and Info-physics, Central South University, Changsha 410083, China

Abstract Rapid urban sprawl and growth led to substantial urban thermal environment changes and influenced the local climate, environment, and quality of life of residents. Taking the Chang-Zhu-Tan urban agglomeration in China as a case, this study firstly identified the spatiotemporal patterns of surface urban heat island intensity (SUHII) and the land use/cover changes (LUCC) based on multi-temporal Landsat TM satellite data over 21 years, and then investigated the relationship between LUCC and SUHII by methods of logistic regression model and centroid shift analysis. The results showed that green spaces (e.g., cropland, forestland) of 899.13 km^2 had been converted to built-up land during the 1994–2015 period, which caused significant urban expansion. The SUHII was the highest for built-up land, high for unused land, low for cropland and grassland, and the lowest for forestland and open water. Many areas experienced extensive rapid urbanization because of the emergence of the urban agglomeration, which resulted in the loss of green spaces and increased SUHI effects over the 21-year study period. In addition, the results of centroid shift analysis found that the growth of SUHII and the expansion of high SUHII areas are closely related to the expansion of an existing urban area in Xiangtan, while the increases of building density and height in Changsha resulted in the decrease of SUHII and spatiotemporal change of high SUHII areas. The analysis of the effects of land use/cover types on the SUHII in this study will contribute to future urban land use allocation for the mitigation of SUHI formation.

Keywords land use/cover change, urbanization, remote sensing, surface urban heat island intensity, centroid shift analysis

Received October 9, 2018; accepted December 25, 2018

E-mail: 210010@csu.edu.cn

1 Introduction

Global urbanization reached a significant level in the second half of the 20th century (Savić et al., 2013). By 2015, more than half of the world's population lived in urban areas (World Health Organization, 2017). Human activities modify the natural environment, with an outcome that reduces natural surfaces, changes urban surface longwave emissions, and releases atmospheric pollutants and waste heat (Zou et al., 2016a, b, 2019; Zhai et al., 2016, 2018; Xu et al., 2018; Jiang et al., 2019). These artificial factors determine a significant local, regional, and global climate (Arnfield, 2003; Kalnay and Cai, 2003; Yuan and Bauer, 2007; Kang et al., 2014). The urban form of urban agglomeration development in China is an irresistible trend of pursuing rapid urbanization. The ideal socioeconomic conditions of urban agglomeration attract rural population migration from rural to urban or suburban areas. These population shifts have affected land use regulations and public policies. The potential interaction between urbanization and urban microclimate change needs to be evaluated because intensive urbanization has a considerable impact on the local microclimate change and the emergence of urban heat islands, which can affect human health and urban comfort (Azevedo and Leal, 2017; Lamarca et al., 2018).

Rapid urbanization may cause urban sprawl, which may result in the change of land use and land cover. In addition, rapid urbanization may densify built-up zones and increase building density and height. The significant LUCC caused by urban agglomeration development will influence and change the ecological environment and urban climate. Owing to the spatial heterogeneity of urban expansion and land-use dynamics (Liu et al., 2010, 2017, 2018), understanding the urban sprawl and growth, as well as the impacts on climate change, is raising concern in the context of global warming.

Remote sensing, with the advantages of low cost and large coverage, has been widely applied to environmental monitoring that can be used to help understand LUCC and rapid urbanization and to estimate the surface urban heat island (SUHI) effect (Li et al., 2014; Fang et al., 2016; Kayet et al., 2016). A remotely sensed thermal infrared (TIR) image can be used to measure land surface temperature (LST) as well as map and monitor the SUHI effect, which has also been used for studying urban climate over a large area (Gluch et al., 2006). Long-term and high-resolution TIR images from Landsat Thematic Mapper (TM)/Enhanced TM Plus (ETM +) are suitable to study the spatiotemporal changes of the SUHI effect and the impacts of LUCC on SUHI intensity (SUHII) with urbanization (Liu and Zhang, 2011).

The formation of SUHI effect is mainly caused by LUCC owing to rapid urban sprawl (Stone et al., 2010). Numerous studies have investigated the relationships between land use/cover type and LST by estimating the surface temperature in different land use/cover patterns (Connors et al., 2013; Wu et al., 2014; Mohan and Kandya, 2015; Cai et al., 2016; Yang et al., 2017). To quantitatively evaluate the effects of urban biophysical compositions on the LST, most studies developed the correlation analysis between the impervious surface area (ISA), normalized difference build-up index (NDBI), the normalized difference vegetation index (NDVI), and LST. These studies found strong positive correlations between the percentage of ISA, NDBI, and LST (Guo et al., 2015), and a strong negative correlation between NDVI and LST (Small, 2001; Wu et al., 2014). However, the spatial and temporal trends of SUHI effect over long periods in different land use/cover patterns have not been adequately elaborated. In addition, it is inappropriate to use the mean LST in different land use/cover types to compare thermal patterns, because an outlier of LST (i.e., extremely low/high LST pixel values) causes the mean to be under- or over-estimated. A logistic regression model that is a qualitative response choice model can evade the issue; it describes the relationship between response variables (e.g., SUHII in response to urbanization) and predictor variables (e.g., land use/cover types) (Hilbe, 2009). This effort will contribute to the understanding of the relationship between different land use/cover types in influencing SUHII.

In addition, urban LST is not only related directly to LUCC because of rapid urban sprawl, but also to the changes of building density and height. High-density and tall buildings within the city obstruct winds that cross through the urban area, thereby aggravating the SUHI effect, and at the same time high-density and tall buildings can also mitigate the SUHI effect by providing a shading effect for reducing incoming solar radiation in summer (Ichinose et al., 2017; Peng et al., 2017). In addition to the understanding of the spatiotemporal impact of LUCC on the SUHI effect, it also needs to explore the impact of the built-up area of the city's becoming progressively more compact. Obviously, more studies are needed on the spatiotemporal influences of urban sprawl and building density and height on the SUHI effect.

In this context, remote sensing, geographic information system, as well as statistical and spatial analysis techniques have been used to monitor, analyze, and study urban thermal environmental change associated with rapid urbanization. The objective of this study is (i) to characterize urban expansion by examining the spatiotemporal change of land use and land cover and to explore the preliminary drivers of expansion, (ii) to investigate the spatiotemporal change of the SUHI effect, and (iii) to study the relationship between the urban built-up areas and thermal patterns. In this study, a logistic regression model and a centroid shift analysis will be used to effectively and accurately evaluate the effect of urban sprawl and growth on the SUHI effect at a fine spatial resolution. The analysis of the effects of land use/cover types on the SUHII will contribute to future urban land use allocation for the mitigation of the SUHI formation. The centroid shift analysis will help track the movements of the urban and high SUHII areas and investigate the potential relationship between urbanization development and SUHI effect.

2 Materials and methods

2.1 Study area and data

The Chang-Zhu-Tan urban agglomeration (the main urban area of Chang-Zhu-Tan) in China is selected as the study area (Fig. 1). It is located in the northeast part of Hunan Province, China, and consists of Changsha City, Changsha County, Xiangtan City, Xiangtan County, Zhuzhou City, and Zhuzhou County (the latitude ranging from 26°N–29°N and longitude being 111°E–114°E) with an area of 8485 km^2, which increased 1100.67 km^2 from 2000 to 2015. The urbanization rate of the urban agglomeration increased from 25.9% to 66.8%, with an annual increase of 2.7% in 2000–2015. The Xiangjiang River runs through the main urban area. The main urban area is under a humid sub-tropical climate with the annual mean temperature of 16°C–18°C and annual mean precipitation of about 1400 mm. Rainfall mostly occurs between April and September. According to the statistics, the study area has experienced accelerated population and economic growths from 1987 to 2015 (Fig. 2). The population and gross domestic product (GDP) have respectively reached 4.80 million and 590.18 billion CNY in Changsha, 1.51 million and 115.92 billion CNY in Zhuzhou, and 1.92 million and 120.63 billion CNY in Xiangtan in 2014. This area has been experiencing a rapid urban expansion due to fast-paced economic growth and urbanization.

The observed air temperature data from a meteorological station were compared with satellite image data from the

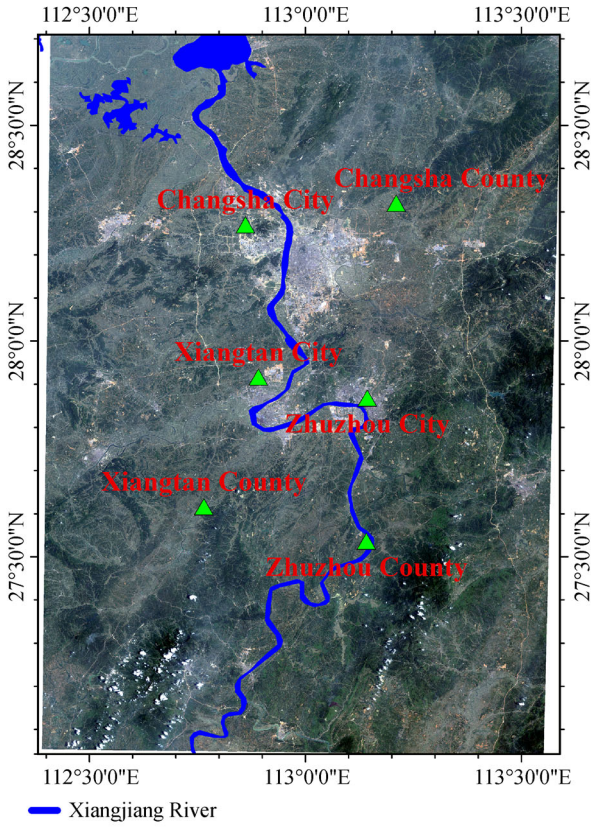

Fig. 1 Study area: the main urban area of Chang-Zhu-Tan, China.

years 1994, 2000, 2006, 2010, and 2015. Five nearly cloud-free Landsat TM/OLI images were selected for this study. Landsat-5 TM images at about 11 am local time on 29 Sept 1994, 13 Sept 2000, 10 Jun 2006, and 26 Jul 2010 were freely downloaded from the website of U.S. Geological Survey, and have 30 m and 120 m spatial resolution for the visible/infrared and thermal bands, respectively. The collected Landsat-8 Operational Land Imager (OLI)/Thermal Infrared Sensor (TIRS) image on 6 Aug 2015 has 100 m spatial resolution for thermal bands 10 and 11, as well as 30 m spatial resolution for the visible/infrared. Due to the unavailability of clear-sky Landsat images, this study used images with slightly different dates to investigate LSTs. The time difference between these images might create some error when comparing LST values from those dates. The *in situ* surface temperatures in 2006 and 2015 were observed to validate the retrieved LSTs. The observed hourly surface temperature from Changsha weather station in 2006 was collected from Hunan province meteorological observatory. In 2015, the surface temperatures from East, North, and South bus stations in Changsha City were observed during the satellite passing the ground stations.

LUCC was detected to examine the effects of urbanization in the Chang-Zhu-Tan urban agglomeration. Land use/cover data with 18 categories in 2000 and 2010 were collected from the Land and Resources Department in Hunan Province. The digital orthophoto maps (DOMs) with 5 m spatial resolution in 2010 and 2015, as well as

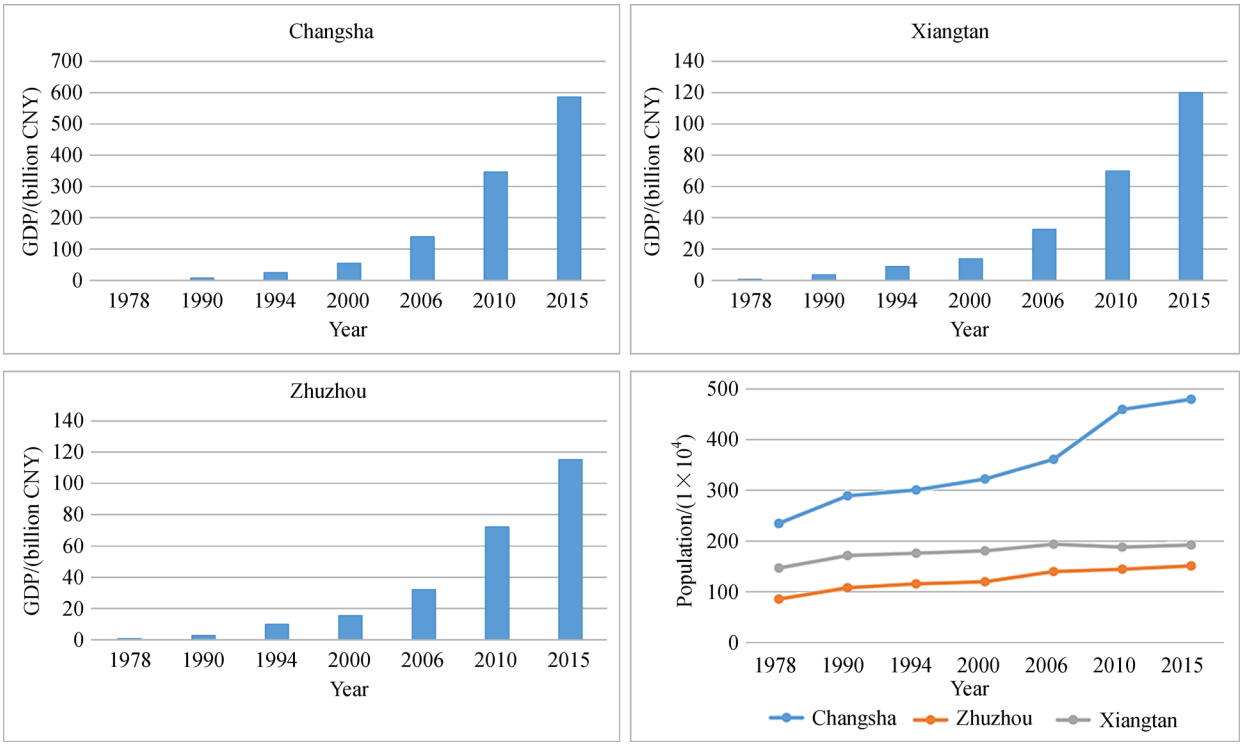

Fig. 2 The changes of GDP and population in Changsha, Zhuzhou, and Xiangtan during the 1987–2015.

multi-temporal nighttime light data from the U.S Air Force Defense Meteorological Satellites Program/Operational Linescan System (DMSP/OLS) in 1994, 2000, and 2006, were acquired to monitor urban expansion for delineating the boundaries between the urban areas and the rural areas.

2.2 Image processing

2.2.1 Land use/cover classification and urban expansion

A land use/cover classification is essential to investigate LUCC from 1994 to 2015. In the study area, land use/cover types were divided into six categories: cropland, forestland, grassland, open water, built-up land, and unused land. The spatial patterns of land use/cover types in 1994, 2006, and 2015 were obtained referring to the color, size, shape, and texture from Landsat false-color composite images using a visual interpretation method through ENVI 5.0. In addition, high spatial resolution Google Earth imagery as an auxiliary data could help identify the category during the process of the visual interpretation. The overall accuracy of the land use/cover maps was 88.84% in 1994, 82.62% in 2006, and 87.27% in 2015, which met the recommended accuracy of land use/cover data (Janssen and Vanderwel, 1994). The pre-existing land use/cover data with 18 categories in 2000 and 2010, meeting the required accuracy, were reclassified and resampled for remaining consistent with category and spatial resolution of land use/cover data in 1994, 2006, and 2015.

The training samples of the urban and surrounding rural areas in 1994, 2000, and 2006 were automatically generated by integrating the indexes retrieved from Landsat remotely sensed images (e.g., spectral information, texture, and impervious surface area) with DMSP/OLS nighttime light data. The support vector machine classifier was then utilized to distinguish the urban areas and the rural areas with reference to the training samples. In addition, a visual interpretation method was required to optimize and delineate the boundary between the urban areas and the rural areas for 1994, 2000, and 2006. The boundary extractions for 2010 and 2015 were developed based on the high spatial resolution DOMs through the visual interpretation method.

2.2.2 Measuring SUHII based on Landsat images

The LSTs in 1994, 2000, 2006, and 2010 were retrieved from the TIR band six of Landsat-5 TM images using the mono-window algorithm (Qin et al., 2001). Landsat 8 TIRS image including two spectrally adjacent thermal bands 10 and 11 in 2015 was acquired to retrieve LST using the split-window algorithm (Rozenstein et al., 2014). The calibration parameters of the satellite sensor and the Planck equation were used to estimate the surface temperature. The parameters including upwelling and downwelling atmospheric radiances, atmospheric transmittance, and surface emissivity were applied to atmospheric and emissivity corrections. The atmospheric transmittance, as well as atmospheric upwelling and downwelling radiances, were obtained using the MODTRAN 4.0 code (Kneizys et al., 1996). Thus, the LST data on 29 Sept 1994, 13 Sept 2000, 10 Jun 2006, 26 Jul 2010, and 6 Aug 2015 were generated and resampled into 30 m spatial resolution. The accuracy assessment of LST was performed using *in situ* LST data. Table 1 shows that the differences between the retrieved LSTs and *in situ* LSTs in 2006 and 2015 were all less than 2°C.

The use of SUHII can reduce the effect of global climate change for the analysis of the microclimate change, because it is the difference in LST between the urban areas and the surrounding rural areas according to the definition of UHI intensity (Oke, 1973; Magee et al., 1999; Kim and Baik, 2005). The SUHIIs in the study were obtained based on the differences between the average LSTs in the urban and rural areas. The differences between the LSTs in all pixels and the mean LST in rural areas were calculated for identifying the spatial patterns of SUHIIs (Schwarz et al., 2011).

2.2.3 Analyzing the effect of LUCC on the SUHII

For a comprehensive view of the impact of the rapid urbanization on the SUHII level, a logistic regression model was used to examine how the LUCC was related to thermal landscape. The use of the logistic regression model was to address the issue that an outlier of LST (i.e., extremely low/high LST in pixel) influenced the comparison of the mean LSTs in different land use/cover types. In the previous study, a logistic regression model had been used to obtain the probability of race (e.g., White, Black) exposure to high air pollution level (Zou et al., 2014; Wong et al., 2016). Logistic regression is commonly utilized to model the probability of a binary outcome such as a logistic function of independent variables. Detailed principles of logistic regression modeling are as follows:

Table 1 Accuracy assessment of retrieved LST (unit: °C)

Year	Weather station	*In situ* LST	Retrieved LST	Difference
2006	Changsha	37.8	36.6	1.2
	East bus station	49.7	51.5	−0.8
2015	North bus station	48.0	49.9	−1.9
	South bus station	49.4	49.3	0.1

$$\text{odds} = P/(1-P), \quad (1)$$

$$P = e^{a+bx}/(1+e^{a+bx}), \quad (2)$$

$$\text{odds ratio} = \frac{p_1/(1-p_1)}{p_2/(1-p_2)}, \quad (3)$$

where odds is the probability of the outcome event to occur (i.e., P) divided by the probability of the event not to occur (i.e., $P/(1–P)$). Odds ratio (OR) indicates the relative value by which the odds of the outcome increase (i.e., OR greater than 1.0) or decrease (i.e., OR less than 1.0) (Hilbe, 2009), e is the exponential constant, equal to 2.71828. P_1 denotes the probability of the case group to occur, P_2 denotes the probability of the control group to occur, x represents the explanatory variables which are either interval–level or "dummy", a and b represent partial regression coefficients of independent variable x.

In this study, the logistic regression model was implemented in SPSS software. In this process, the SUHII levels (<0°C, 0°C–4°C, 4°C–8°C, 8°C–12°C, 12°C–16°C, and >16°C) were dichotomized as the dependent variables. The land use/cover types (cropland, forestland, grassland, open water, built-up land, and unused land) were selected as independent variables. In addition, the reference categories in SUHII levels and land use/cover patterns should also be determined to obtain the relative risk.

The centroid shift analyses of the high SUHII (>4°C) and urban areas in Changsha, Xiangtan, and Zhuzhou were conducted to examine the dynamic changes in thermal patterns and urbanization between 1994 and 2015. The centroid shift analysis can explore the influences of urban sprawl and growth on the SUHI effect. The mean center tool is a measure of central tendency in ArcGIS (Scott and Janikas, 2010). The mean center is the average x and y coordinates of all pixels in the high SUHII areas or the urban areas. The coordinates of the centroid are calculated by Eqs. (4) and (5) (Scott and Janikas, 2010).

$$X_t = \sum_{i=1}^{n}(A_{ti} \times X_{ti}) / \sum_{i=1}^{n} A_{ti}, \quad (4)$$

$$Y_t = \sum_{i=1}^{n}(A_{ti} \times Y_{ti}) / \sum_{i=1}^{n} A_{ti}, \quad (5)$$

where X_{ti} and Y_{ti} are the coordinates for each pixel of the high SUHII area or the urban area in the t year, n is the total number of pixels, and A_{ti} is the area of each pixel in the t year. The result of the X_t and Y_t coordinate pair is the location of the high SUHII area-based weighted mean center, which is called the SUHII area centroid, and the urban area-based weighted mean center is called the urban area centroid. The centroids between 1994 and 2015 were used to investigate how the spatial pattern of the high SUHII area changes with urban sprawl and growth.

3 Results

3.1 Spatiotemporal patterns of LUCC and urban sprawl

The land use dynamics and temporal changes in the urban agglomeration from 1994–2015 are shown in Fig. 3. The land use/cover maps including six categories (cropland, forestland, grassland, open water, built-up land, and unused land) between 1994 and 2015, which were identified to characterize the biophysical features of the urban landscape. It indicates that built-up areas were more concentrated in the central parts of the Changsha, Zhuzhou, and Xiangtan in 1994 (Figs. 3(a) and 4(a)) but expanded in different directions over time (Figs. 3(b)–3(e) and Figs. 4(b)–4(e)). The area of cropland had a continuously decreasing trend, especially from 2006 onwards, while the built-up land was experiencing a continued expansion during this period. Table 2 shows that the area for cropland decreased by 823.55 km^2 from 1994 to 2015. By contrast, the area of built-up land increased by 899.13 km^2 during this period. The overall growth in the built-up land was mostly attributed to the loss of cropland and forestland. Urban expansion and shrinking cropland were significantly presented in the study area. To investigate the effect of urbanization on the SUHI effect, the boundaries between urban and surrounding rural areas in Changsha, Xiangtan, and Zhuzhou between 1994 and 2015 were delineated as shown in Fig. 3. The considerable increases occurred in the urban areas during the 1994–2015 period, i.e., 432.67% of the total area in Changsha, 88.36% of the total area in Zhuzhou, and 150.95% of the total area in Xiangtan. The urban agglomeration experienced considerable urbanization in multiple directions during the study period.

3.2 Spatiotemporal variations of SUHIIs between 1994 and 2015

Figure 5 shows the monthly average air temperature in the period from 1994 to 2010 in Changsha. The highest temperatures occur between June and September. The monthly average maximum and minimum air temperatures between June and September in 2015 exhibit small variations. A small variation in temperature was observed in the studied months (approximately 3.2°C in maximum air temperature and 3.0°C in minimum air temperature). If the first half month in September was selected to compare the air temperature between June and September, the changes in temperature were approximately 1.7°C in maximum air temperature and 2.1°C in minimum air temperature.

Figure 6 shows the spatial distributions of the LSTs between 1994 and 2015. The significant LST gradients between the urban areas and the surrounding rural areas in Changsha, Xiangtan, and Zhuzhou were observed during

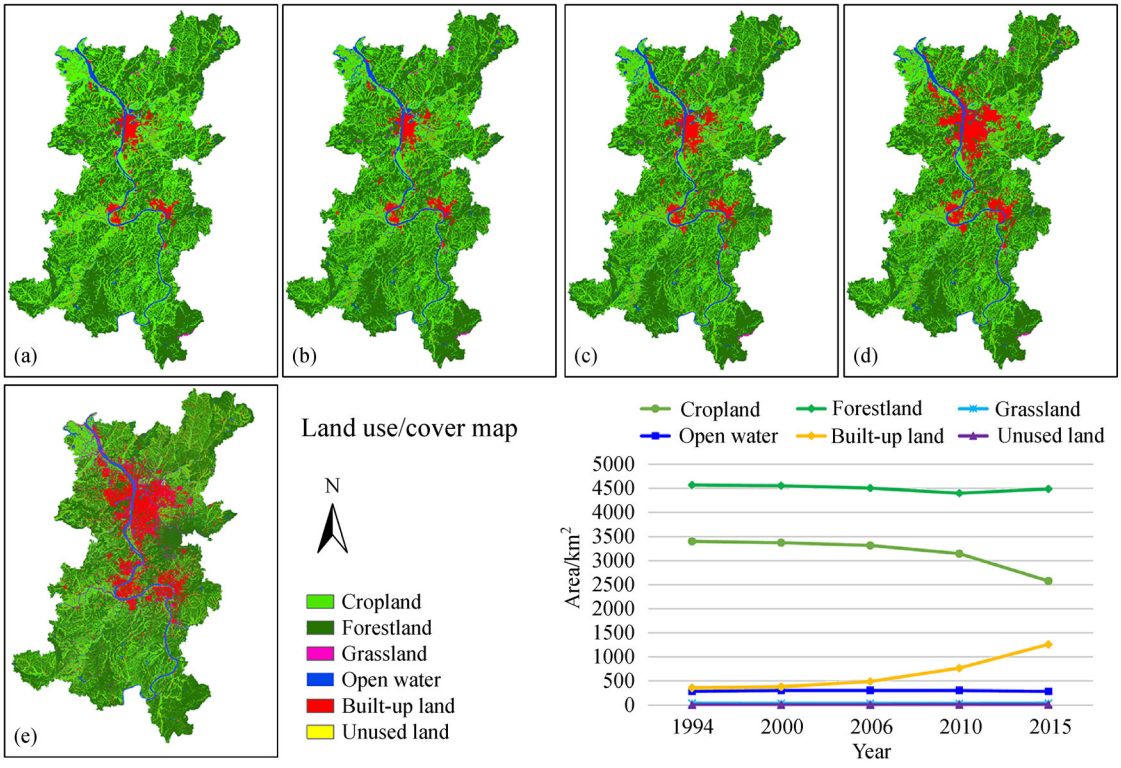

Fig. 3 Land use/cover: (a) 1994, (b) 2000, (c) 2006, (d) 2010, and (e) 2015.

this period. In response to rapid urbanization and shrinking cropland, Changsha City, Xiangtan City, and Zhuzhou City exhibited the higher LST and appeared the relatively fixed and expanding area. By contrast, Changsha County, Xiangtan County, and Zhuzhou County show the relative lower variation in the LST because of larger vegetation coverage. The inter-annual variation in SUHII is shown in Table 3, i.e., the SUHII in the study area increased significantly from 1994 to 2015. The SUHII was classified into six levels (<0°C, 0°C–4°C, 4°C–8°C, 8°C–12°C, 12°C–16°C, and >16°C), and the size of each class interval is 4°C with reference to the SUHII of the study area in Table 3. Figure 7 shows the overall spatial patterns of the SUHII from 1994 to 2015, which can be used to analyze the correlation with the LUCC. Over the past 20 years, dramatic changes have occurred in land use/cover patterns, which exert a great influence on the thermal environment. The highest SUHII zones were found inside the urban area, and the higher or high zones had a scattered distribution which looked like an isolated heat island. Then, the isolated heat island had been merged into the central area gradually over time for creating a larger area. The significant decreased and increased areas occurred in SUHII (<0°C) and SUHII (0°C–4°C) levels respectively from 1994 to 2006. After that, the trend was not obvious. The trends of areas of the SUHII (4°C–8°C), SUHII (8°C–12°C), SUHII (12°C–16°C), and SUHII (>16°C) levels were similar and increased significantly from 1994 to 2015, especially from 2006 onwards. Owing to the similar changes and small areas of these SUHII levels, the four levels can be integrated into a high SUHII level. The centroid shift analysis of the high SUHII (>4°C) areas with urbanization were then established.

3.3 Change analysis of SUHIIs by the spatiotemporal patterns of LUCC

The probability the high SUHII occurring in land use/cover patterns, as well as the centroid shift analyses of the high SUHII and urban areas, was studied for investigating the effects of LUCC on the SUHII and further showing their explicit spatial characteristics. The ORs were computed using SUHII levels as the dependent variables, and the land use/cover types as independent variables to further determine the change patterns of high SUHII in the different land use/cover types. The SUHII (<0°C) level and cropland were regarded as the reference category respectively owing to the significant decrease of cropland area. Table 4 shows ORs of SUHII levels in land use/cover patterns, and no data is deemed to be statistically insignificant. The table shows that the significant SUHI effect in 1994 focused on the SUHII (0°C–4°C) and SUHII (4°C–8°C) levels, and the high SUHII was most likely to occur in the built-up land owing to the large OR value. During the 1994–2015 period, the high SUHII was also mainly focused on the built-up land compared to cropland,

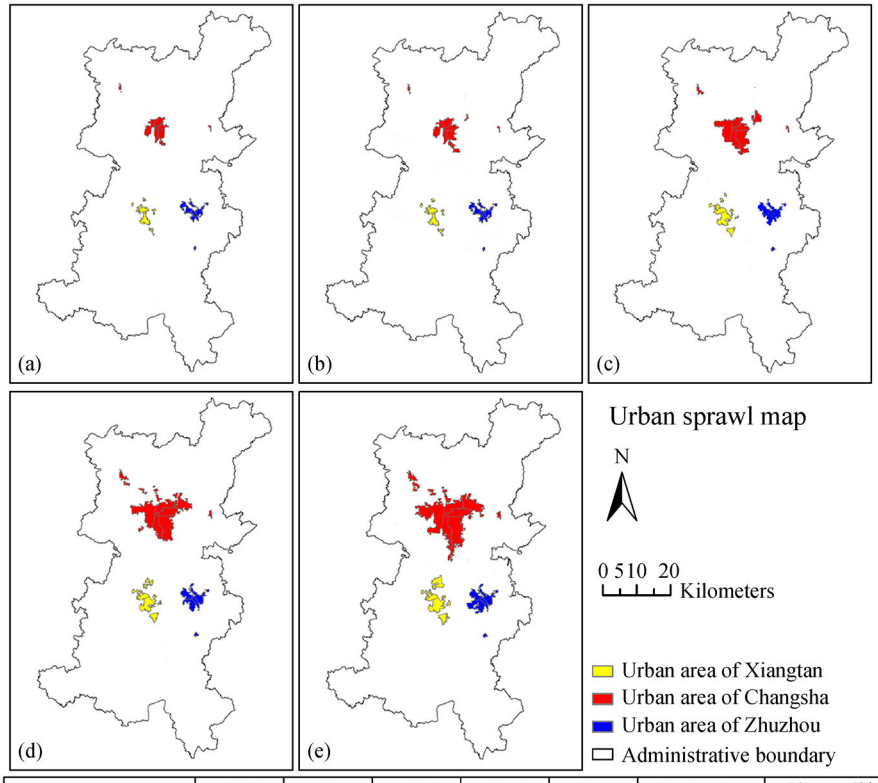

	1994	2000	2006	2010	2015	1994–2015	Change/%
Urban area of Xiangtan	62.97	77.51	154.57	232.51	335.29	272.32	+432.67
Urban area of Changsha	26.89	28.72	44.10	51.21	67.48	40.59	+150.95
Urban area of Zhuzhou	38.23	40.85	53.84	59.47	72.01	33.78	+88.36
Total area	128.09	147.08	252.51	343.19	474.78	346.69	+270.66

Fig. 4 Urban sprawl: (a) 1994, (b) 2000, (c) 2006, (d) 2010, and (e) 2015.

Table 2 The change of land use and cover between 1994 and 2015 (unit: km^2)

Land use/cover type	1994–2000	2000–2006	2006–2010	2010–2015	1994–2015
Cropland	−26.92	−58.39	−170.51	−567.73	−823.55
Forestland	−14.79	−46.70	−108.96	+90.41	−80.04
Grassland	−0.10	−0.38	−0.63	+2.81	+1.7
Open water	+18.30	−0.57	−1.82	−16.49	−0.58
Built-up land	+23.46	+105.73	+279.47	+490.47	+899.13
Unused area	+0.05	+0.31	+2.44	−0.33	+2.47

especially SUHII (>4°C) level, whereas the low SUHII was observed in the areas of forestland and open water. The high SUHIIs in 2010 and 2015 were also exhibited in the unused land. The effect of grassland on the SUHII compared to cropland had no significant regularity. In 2000 and 2015, cropland was more significant than grassland in cooling the surface temperature, whereas the grassland had the cooling benefit in 2010.

Figure 8 shows the centroid locations and shifts of the urban and high SUHII (>4°C) areas from 1994 to 2015. Overall, the centroid shifts in urban areas and high SUHII areas over time occurred from east to west in Changsha, from southwest to northeast in Zhuzhou, and from north to south in Xiangtan. The trends of centroid shifts between urban areas and high SUHII areas in Xiangtan during this period were the most similar. Table 5 shows that the shortest distance of the centroids between the urban areas and high SUHII areas was 0.33 km in 2006 and occurred in Xiangtan. The SUHII of Xiangtan increased significantly from 1994 to 2015, and was larger than Changsha and Zhuzhou in 2010 and 2015. These indicate that the growth of SUHII and the expansion of high SUHII areas are closely related to the expansion of an existing urban area in Xiangtan. It also demonstrated that the existence of SUHI

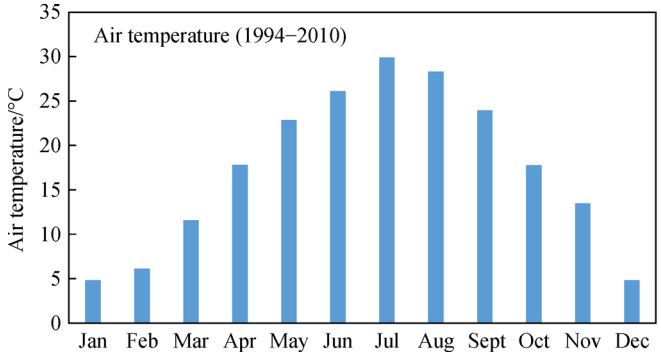

Monthly average air temperature in 2015

Month	T_{max}	T_{min}
Jun	30.3	24.2
Jul	30.2	24.6
Aug	31.9	25.1
Sept	28.7	22.1
1 Sept—15 Sept	30.5	23.0

Fig. 5 Monthly average air temperature for 1994–2015.

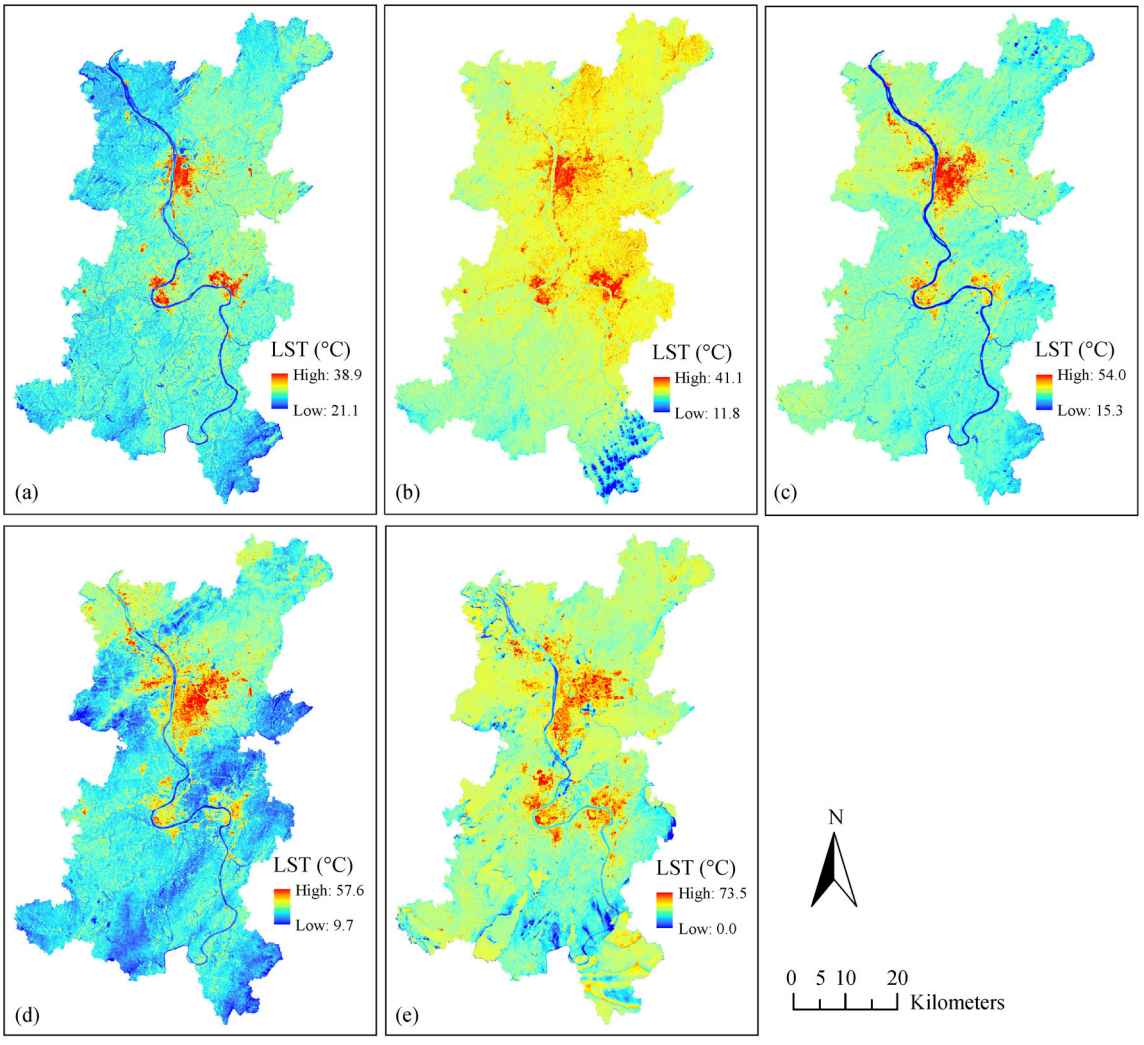

Fig. 6 Spatial distributions of LSTs retrieved from Landsat images. (a) 1994, (b) 2000, (c) 2006, (d) 2010, and (e) 2015.

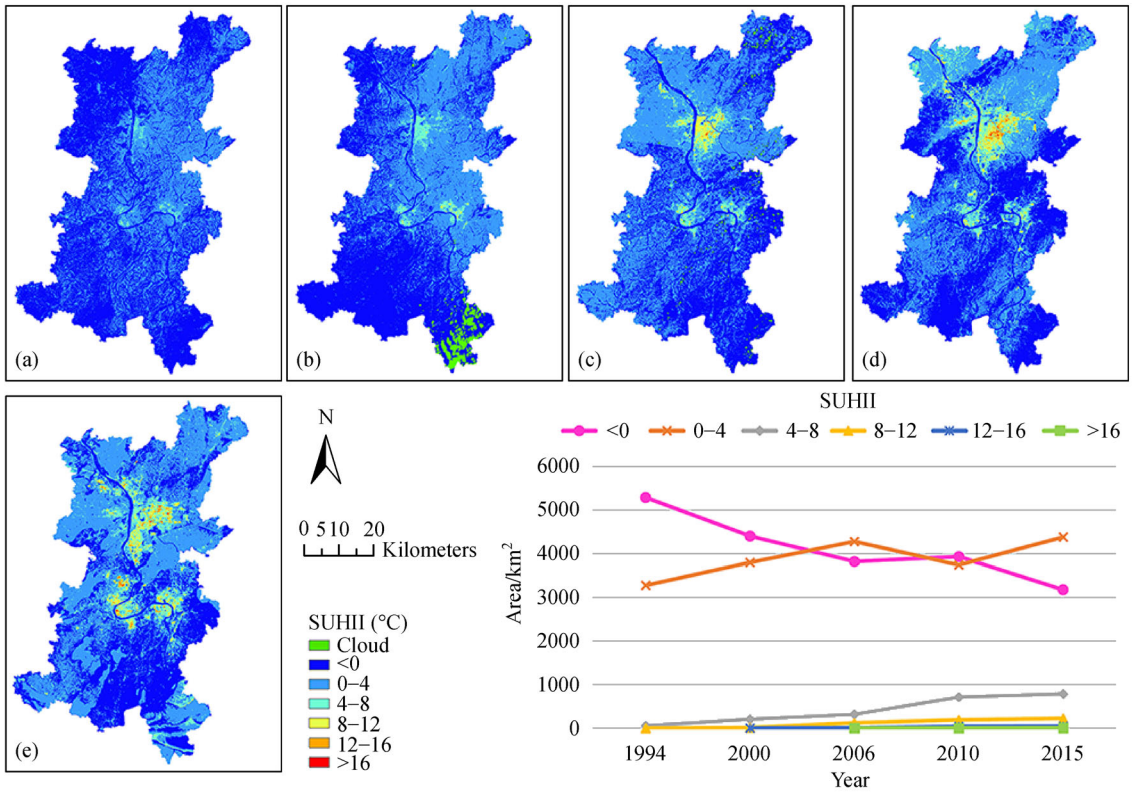

Fig. 7 Spatial patterns of SUHIIs. (a) 1994, (b) 2000, (c) 2006, (d) 2010, and (e) 2015.

Table 3 Variation of SUHII between 1994 and 2015 (unit: °C)

Year	Mean LST	Mean LST in urban areas	Mean LST in rural areas	SUHII
1994	26.6	29.8	26.5	3.3
2000	24.9	29.5	24.8	4.7
2006	30.6	36.2	30.4	5.8
2010	33.5	39.7	33.2	5.9
2015	39.9	46.7	39.5	7.2

effect is difficult to refute as it grows simultaneously with the expansion of the urban area that causes the change in surface temperature. Table 5 shows that the maximum distance of centroids between the urban areas and the high SUHII areas was 2.15 km in Changsha for the year 2015. The SUHII increased in Xiangtan and Zhuzhou, but decreased in Changsha from 2006 onwards.

4 Discussion

Urban agglomeration has become one of the most distinguishing features of recent urbanization worldwide (Wu, 2014). This study investigated the spatiotemporal distributions of SUHII and urbanization, and studied the effects of urban sprawl and growth on the SUHI effect in the Chang-Zhu-Tan urban agglomerations. The results showed that the area of cropland had a continuously decreasing trend, especially from 2006 onwards, while the built-up land was experiencing a continued expansion. This was because the government of Hunan Province proposed a regional planning to build Chang-Zhu-Tan urban agglomeration in October 2005. Changsha, Xiangtan, and Zhuzhou began to develop quickly for merging into the urban agglomeration. Recently, most studies found that the built-up area increases the SUHII dramatically while the vegetation can cool the environment, which was also demonstrated in Chang-Zhu-Tan main urban area (Zeng et al., 2010; Lan and Ming, 2018). Similar to previous finding, our study found that the high SUHII was mainly focused on the built-up land compared to cropland, whereas the low SUHII was observed in the areas of forestland and open water. These findings highlight the importance of vegetation cover and open water for urban

Table 4 ORs and 95% confidence intervals of SUHII levels in land use/cover patterns

Year	SUHII level	Forestland	Grassland	Open water	Built-up land	Unused land
1994	SUHII (0°C–4°C)	2.28 (2.27, 2.28)	0.88 (0.86, 0.90)	0.01 (0.01, 0.02)	3156.24 (2488.46, 4003.21)	0.38 (0.35, 0.41)
	SUHII (4°C–8°C)	0.32 (0.26, 0.40)	4.22 (2.67, 6.67)	1.64 (1.37, 1.95)	2301503.56 (1786053.15, 2965711.66)	8.29 (3.70, 18.56)
	SUHII (8°C–12°C)	—	—	—	—	—
	SUHII (12°C–16°C)	—	—	—	—	—
	SUHII (> 16°C)	—	—	—	—	—
2000	SUHII (0°C–4°C)	1.73 (1.73, 1.74)	2.79 (2.72, 2.87)	0.30 (0.30, 0.31)	6.91 (6.82, 6.99)	1.10 (1.02, 1.18)
	SUHII (4°C–8°C)	0.70 (0.69, 0.72)	5.19 (4.79, 5.62)	0.48 (0.46, 0.51)	356.38 (350.38, 362.49)	—
	SUHII (8°C–12°C)	0.56 (0.45, 0.72)	—	—	3632.36 (3160.61, 4174.52)	—
	SUHII (12°C–16°C)	—	—	—	2661.43 (1185.35, 5975.6)	—
	SUHII (> 16°C)	—	—	—	—	—
2006	SUHII (0°C–4°C)	1.16 (1.16, 1.16)	1.52 (1.48, 1.56)	0.17 (0.17, 0.17)	4.81 (4.75, 4.88)	0.23 (0.21, 0.25)
	SUHII (4°C–8°C)	0.61 (0.60, 0.62)	0.27 (0.23, 0.32)	0.39 (0.38, 0.40)	119.02 (117.32, 120.74)	0.16 (0.11, 0.24)
	SUHII (8°C–12°C)	0.28 (0.27, 0.29)	—	0.50 (0.48, 0.53)	314.01 (307.65, 320.51)	0.16 (0.07, 0.39)
	SUHII (12°C–16°C)	0.05 (0.04, 0.06)	—	0.19 (0.15, 0.23)	242.77 (232.08, 253.94)	—
	SUHII (> 16°C)	0.20 (0.15, 0.26)	—	0.08 (0.03, 0.22)	142.64 (124.36, 163.61)	—
2010	SUHII (0°C–4°C)	0.94 (0.93, 0.94)	0.53 (0.52, 0.54)	0.31 (0.30, 0.31)	4.88 (4.82, 4.93)	5.15 (4.72, 5.61)
	SUHII (4°C–8°C)	0.75 (0.74, 0.75)	0.34 (0.32, 0.36)	0.48 (0.47, 0.49)	65.58 (64.81, 66.37)	13.33 (12.10, 14.68)
	SUHII (8°C–12°C)	0.56 (0.55, 0.58)	0.01 (0.00, 0.04)	0.76 (0.73, 0.80)	333.90 (327.82, 340.08)	54.53 (48.37, 61.47)
	SUHII (12°C–16°C)	0.33 (0.30, 0.36)	—	1.57 (1.40, 1.75)	912.36 (867.16, 959.90)	40.21 (27.94, 57.88)
	SUHII (> 16°C)	0.06 (0.01, 0.24)	—	6.59 (3.85, 11.30)	5741.50 (3903.96, 8443.94)	—
2015	SUHII (0°C–4°C)	0.76 (0.75, 0.76)	1.64 (1.59, 1.68)	0.15 (0.15, 0.15)	3.20 (3.18, 3.22)	0.56 (0.53, 0.59)
	SUHII (4°C–8°C)	0.38 (0.37, 0.38)	1.78 (1.69, 1.87)	0.09 (0.08, 0.09)	45.38 (44.97, 45.80)	2.21 (2.03, 2.41)
	SUHII (8°C–12°C)	0.40 (0.38, 0.42)	7.21 (6.19, 8.39)	0.03 (0.02, 0.05)	778.32 (750.05, 807.67)	12.39 (10.05, 15.28)
	SUHII (12°C–16°C)	0.18 (0.14, 0.25)	5.88 (2.89, 11.97)	0.19 (0.10, 0.36)	2916.02 (2496.44, 3406.13)	48.40 (30.36, 77.18)
	SUHII (> 16°C)	0.19 (0.09, 0.37)	—	11.98 (7.91, 18.13)	2879.05 (1986.49, 4172.65)	—

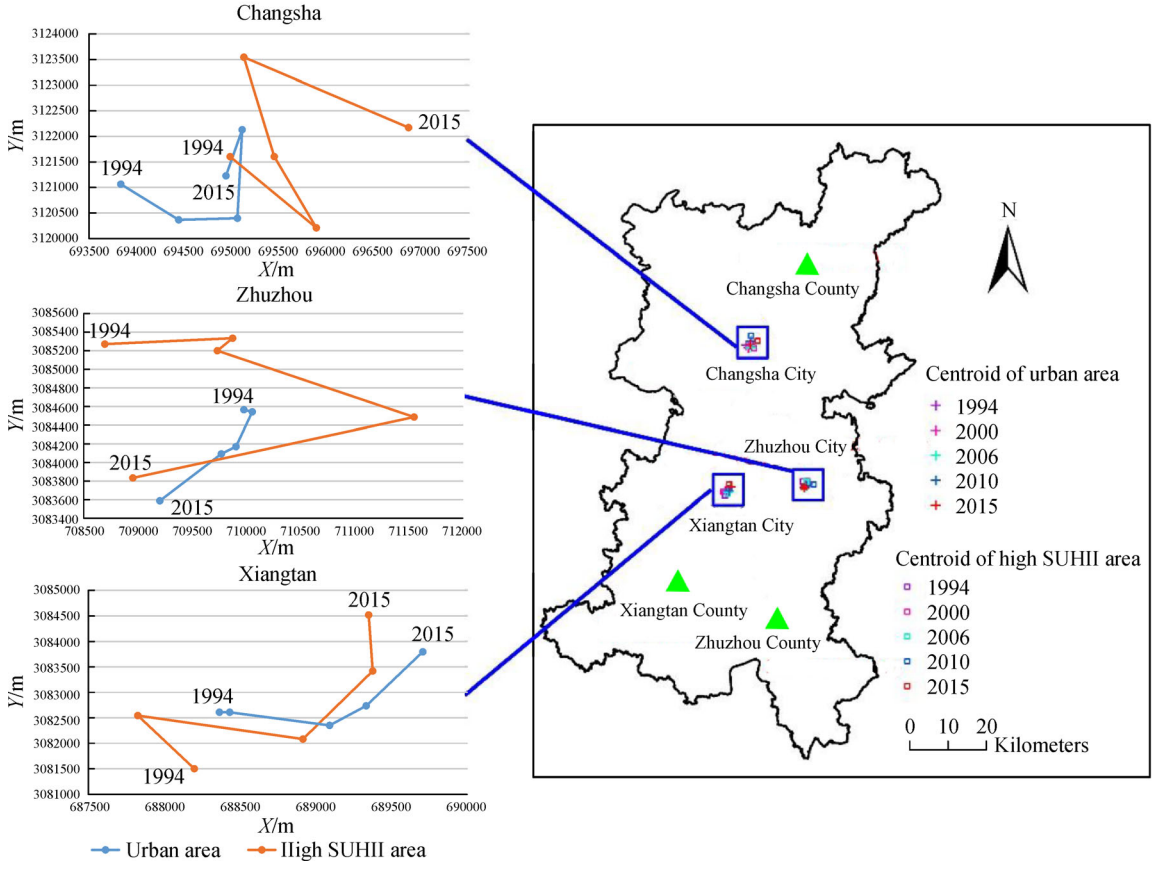

Fig. 8 Centroid locations and shifts of the urban and high SUHII areas between 1994 and 2015.

Table 5 The SUHIIs and centroid distance between urban areas and high SUHII areas

City	Centroid distance/km					SUHII/°C				
	1994	2000	2006	2010	2015	1994	2000	2006	2010	2015
Changsha	1.27	1.45	1.27	1.43	2.15	3.1	3.8	6.2	5.9	4.5
Zhuzhou	1.47	0.81	1.04	1.83	0.35	3.3	5.4	4.6	5.1	6.9
Xiangtan	1.09	0.61	0.33	0.68	0.80	3.6	5.5	5.1	6.2	7.8

comfort and confirm that urban areas have a significant impact on the conditions in the surrounding environment and the existence of urban microclimates (urban heat island and urban cool island).

Different from the previous studies, this study identified the spatiotemporal patterns of the SUHII and the LUCC over the past 21 years, and found that the areas of the high SUHII (4°C–8°C), SUHII (8°C–12°C), SUHII (12°C–16°C), and SUHII (> 16°C) levels increased significantly in response to the rapid urban sprawl of the study area. The logistic regression model compared to the previous liner regression analysis and comparative method is a new tempt for studying the relationship between the SUHII and LUCC. This may affect the result to some extent and can be adopted in contribution analysis of impact factors. The centroid shift analysis method used from this study might provide new insights for such future efforts. According to the centroid shift analysis, the decreased SUHII and the largest centroid distance between the urban areas and the high SUHII areas during the period 1994–2015 occurred in Changsha. This is because other factors such as the anthropogenic heat flux and shading effects of buildings except urban sprawl may also play important roles in affecting the SUHII. For instance, heat releases caused by the extensive air conditioning usage in summer can exaggerate the SUHII (Wang et al., 2015). Meanwhile, high-density and high-rise buildings can easily form shadows, and thus decrease the LST in urban areas (Du et al., 2016; Peng et al., 2017). Therefore, the centroid shift analysis can help investigate the spatiotemporal character-

istics of urban development according to the move of the SUHII hotspot area; at the same time urban sprawl or the increases of building density and height can also help ascertain the spatiotemporal change of the high SUHII areas. Several limitations should be discussed in this study. LST data of a high temporal resolution should be used to investigate the effects of LUCC on the thermal environment at a high spatial resolution; it provides more effective and accurate information for policy-makers and urban planners. However, remote sensing images were limited by the revisit period and cloud contamination. The spatiotemporal changes of nighttime SUHIIs with urbanization were not studied. Although images from Advanced Spaceborne Thermal Emission and Reflection Radiometer (ASTER) and Moderate Resolution Imaging Spectroradiometer (MODIS) were widely used to obtain nighttime SUHII, both ASTER and MODIS were launched in 1999, and images from MODIS had a large spatial scale. In addition, more detailed land use/cover types (e.g., paddy land, dry land, woodland, residential land, and commercial land) should also be considered. When local climate knowledge is considered in pursuing urbanization, smart design needs to be stressed and studied for improving the local urban climate. Some possible countermeasures should be proposed. For example, Emmanuel and Fernando (2007) found that the best thermal comfort was concentrated in the high-density building zone during daytime. Santamouris (2013) found that cool pavements contributed significantly to the decrease of urban temperature. Peng et al. (2017) proposed that daytime thermal distress can be reduced by enhancing the shading effects, and by improving air ventilation based on more E-W horizon corridors in pursuing a compact urban form. Thus, understanding the relationship between urban morphology and urban microclimate is necessary to urban planners for a quality urban thermal environment in a future study.

5 Conclusions

In the study, an integrated approach including remote sensing technique, GIS, and statistical analysis was employed to analyze dynamics of LUCC and thermal characteristics in response to the rapid urban expansion and growth in the Chang-Zhu-Tan urban agglomeration between 1994 and 2015. It is obvious that hotspots of urban micro-climate exist and expand because of the presence and development of urban agglomeration from 1994 to 2015. In detail, the decreases in cropland, grassland, and forestland, together with the increased size of buildings, resulted in increases of SUHII and the expansion of high SUHII area over the 21-year study period. Meanwhile, high-rise and high-density buildings contribute to the formation of shadows, and thus decrease the SUHII and change the spatial movement of the high SUHII area in urban areas. The centroid shift analysis provides new insights for studying the spatiotemporal relationship between the high SUHII area and the urban sprawl and growth. It can help explore the spatiotemporal characteristics of urban development referring to the movement of the high SUHII area. At the same time, urban sprawl or the increases of building density and height can also help ascertain the spatiotemporal change of the high SUHII areas. The findings in this study can help improve planning and decision making in the urban environment management and future studies about the adverse effects of SUHIs in urban areas.

Acknowledgements This work was supported by the National Natural Science Foundation of China (No. 41871317), National Social Science Foundation of China (No.15BJY051), the Open Fund of University Innovation Platform, Hunan (No. 15K132), and National Geographic Conditions Monitoring in Hunan (HNGQJC2015-03).

References

Arnfield A J (2003). Two decades of urban climate research: a review of turbulence, exchanges of energy and water, and the urban heat island. Int J Climatol, 23(1): 1–26

Azevedo I, Leal V M S (2017). Methodologies for the evaluation of local climate change mitigation actions: a review. Renew Sustain Energy Rev, 79: 681–690

Cai Y, Zhang H, Zheng P, Pan W (2016). Quantifying the impact of land use/land cover changes on the urban heat island: a case study of the natural wetlands distribution area of Fuzhou City, China. Wetlands, 36(2): 285–298

Connors J P, Galletti C S, Chow W T L (2013). Landscape configuration and urban heat island effects: assessing the relationship between landscape characteristics and land surface temperature in Phoenix, Arizona. Landsc Ecol, 28(2): 271–283

Du H, Wang D, Wang Y, Zhao X, Qin F, Jiang H, Cai Y (2016). Influences of land cover types, meteorological conditions, anthropogenic heat and urban area on surface urban heat island in the Yangtze River Delta Urban Agglomeration. Sci Total Environ, 571: 461–470

Emmanuel R, Fernando H J S (2007). Urban heat islands in humid and arid climates: role of urban form and thermal properties in Colombo, Sri Lanka and Phoenix, USA. Clim Res, 34(3): 241–251

Fang X, Zou B, Liu X, Sternberg T, Zhai L (2016). Satellite-based ground $PM_{2.5}$ estimation using timely structure adaptive modeling. Remote Sens Environ, 186: 152–163

Gluch R, Quattrochi D A, Luvall J C (2006). A multi-scale approach to urban thermal analysis. Remote Sens Environ, 104(2): 123–132

Guo G, Wu Z, Xiao R, Chen Y, Liu X, Zhang X (2015). Impacts of urban biophysical composition on land surface temperature in urban heat island clusters. Landsc Urban Plan, 135: 1–10

Hilbe J M (2009). Logistic Regression Models. Chapman and Hall/CRC Press, 220–225

Ichinose T, Lei L, Lin Y (2017). Impacts of shading effect from nearby buildings on heating and cooling energy consumption in hot summer and cold winter zone of China. Energy Build, 136(1): 199–210

Janssen L L F, Vanderwel F J M (1994). Accuracy assessment of satellite

derived land-cover data: a review. Photogramm Eng Remote Sensing, 60(4): 419–426

Jiang X, Zou B, Feng H, Tang J, Tu Y, Zhao X (2019). Spatial distribution mapping of Hg contamination in subclass agricultural soils using GIS enhanced multiple linear regression. J Geochem Explor, 196: 1–7

Kalnay E, Cai M (2003). Impact of urbanization and land-use change on climate. Nature, 423(6939): 528–531

Kang H, Zhu B, Zhu T, Sun J, Ou J (2014). Impact of megacity Shanghai on the urban heat-island effects over the downstream city Kunshan. Boundary-Layer Meteorol, 152(3): 411–426

Kayet N, Pathak K, Chakrabarty A, Sahoo S (2016). Spatial impact of land use/land cover change on surface temperature distribution in Saranda Forest, Jharkhand. Model Earth Syst Environ, 2(3): 127

Kim Y H, Baik J J (2005). Spatial and temporal structure of the urban heat island in Seoul. J Appl Meteorol, 44(5): 591–605

Kneizys F X, Abreu L W, Anderson G P, Chetwynd J H, Shettle E P, Berk A, Bernstein L S, Robertson D C, Acharya P K, Rothman L A, Selby J E A, Gallery W O, Clough S A (1996). The MODTRAN 2/3 report & LOWTRAN 7 model, F19628-91-C-0132. Phillips Laboratory Hanscom AFB, Bedford

Lamarca C, Qüense J, Henríquez C (2018). Thermal comfort and urban canyons morphology in coastal temperate climate, Concepción, Chile. Urban Climate, 23: 159–172

Lan C, Ming L I (2018). Spatial-temporal feature of urban heat island in Changzhutan main urban area and the relationship with land use change. Geomatics & Spatial Information Technology, 41(4): 84–89 (in Chinese)

Li H, Sun D, Yu Y, Wang H, Liu Y, Liu Q, Du Y, Wang H, Cao B (2014). Evaluation of the VIIRS and MODIS LST products in an arid area of Northwest China. Remote Sens Environ, 142(1): 111–121

Liu L, Zhang Y (2011). Urban heat island analysis using the Landsat TM data and ASTER data: a case study in Hong Kong. Remote Sens, 3 (7): 1535–1552

Liu X, Hu G, Chen Y, Li X, Xu X, Li S, Pei F, Wang S (2018). High-resolution multi-temporal mapping of global urban land using Landsat images based on the Google Earth Engine Platform. Remote Sens Environ, 209: 227–239

Liu X, Li X, Shi X, Zhang X, Chen Y (2010). Simulating land-use dynamics under planning policies by integrating artificial immune systems with cellular automata. Int J Geogr Inf Sci, 24(5): 783–802

Liu X, Liang X, Li X, Xu X, Ou J, Chen Y, Li S, Wang S, Pei F (2017). A future land use simulation model (FLUS) for simulating multiple land use scenarios by coupling human and natural effects. Landsc Urban Plan, 168: 94–116

Magee N, Curtis J, Wendler G (1999). The urban heat island effect at Fairbanks, Alaska. Theor Appl Climatol, 64(1–2): 39–47

Mohan M, Kandya A (2015). Impact of urbanization and land-use/land-cover change on diurnal temperature range: a case study of tropical urban airshed of India using remote sensing data. Sci Total Environ, 506– 507: 453–465

Oke T R (1973). City size and the urban heat island. Atmos Environ, 7 (8): 769–779

Peng F, Wong M S, Ho H C, Nichol J, Chan P W (2017). Reconstruction of historical datasets for analyzing spatiotemporal influence of built environment on urban microclimates across a compact city. Build Environ, 123: 649–660

Qin Z, Karnieli A, Berliner P (2001). A mono-window algorithm for retrieving land surface temperature from Landsat TM data and its application to the Israel-Egypt border region. Int J Remote Sens, 22 (18): 3719–3746

Rozenstein O, Qin Z, Derimian Y, Karnieli A (2014). Derivation of land surface temperature for Landsat-8 TIRS using a split window algorithm. Sensors (Basel), 14(4): 5768–5780

Santamouris M (2013). Using cool pavements as a mitigation strategy to fight urban heat island—a review of the actual developments. Renew Sustain Energy Rev, 26(10): 224–240

Savić S, Unger J, Gál T, Milošević D, Popov Z (2013). Urban heat island research of Novi Sad (Serbia): a review. Geogr Pannon, 17(1): 32–36

Schwarz N, Lautenbach S, Seppelt R (2011). Exploring indicators for quantifying surface urban heat islands of European cities with MODIS land surface temperatures. Remote Sens Environ, 115(12): 3175–3186

Scott L M, Janikas M V (2010). Spatial Statistics in ArcGIS. Handbook of Applied Spatial Analysis, 27–41

Small C (2001). Estimation of urban vegetation abundance by spectral mixture analysis. Int J Remote Sens, 22(7): 1305–1334

Stone B, Hess J J, Frumkin H (2010). Urban form and extreme heat events: are sprawling cities more vulnerable to climate change than compact cities? Environ Health Perspect, 118(10): 1425–1428

Wang X, Sun X, Tang J, Yang X (2015). Urbanization-induced regional warming in Yangtze River Delta: potential role of anthropogenic heat release. Int J Climatol, 35(15): 4417–4430

Wong M S, Peng F, Zou B, Shi W Z, Wilson G J (2016). Spatially analyzing the inequity of the Hong Kong urban heat island by socio-demographic characteristics. Int J Env Res Pub He, 13(3): 317

World Health Organization (2017). Global Health Observatory (GHO) data. World Health Organization, Geneva

Wu H, Ye L P, Shi W Z, Clarke K C (2014). Assessing the effects of land use spatial structure on urban heat islands using HJ-1B remote sensing imagery in Wuhan, China. International Journal of Applied Earth Observation and Geoinformation, 32(1): 67–78

Wu J (2014). Urban ecology and sustainability: the state-of-the-science and future directions. Landsc Urban Plan, 125: 209–221

Xu S, Zou B, Shafi S, Sternberg T (2018). A hybrid Grey-Markov/ LUR model for PM_{10} concentration prediction under future urban scenarios. Atmos Environ, 187: 401–409

Yang C, He X, Yan F, Yu L, Bu K, Yang J, Chang L, Zhang S (2017). Mapping the influence of land use/land cover changes on the urban heat island effect—a case study of Changchun, China. Sustainability, 9(2): 312

Yuan F, Bauer M E (2007). Comparison of impervious surface area and normalized difference vegetation index as indicators of surface urban heat island effects in Landsat imagery. Remote Sens Environ, 106(3): 375–386

Zeng Y, Huang W, Zhan F B, Zhang H, Liu H (2010). Study on the urban heat island effects and its relationship with surface biophysical characteristics using MODIS imageries. Geo Spat Inf Sci, 13(1): 1–7

Zhai L, Li S, Zou B, Sang H, Fang X, Xu S (2018). An improved geographically weighted regression model for $PM_{2.5}$ concentration estimation in large areas. Atmos Environ, 181: 145–154

Zhai L, Zou B, Fang X, Luo Y, Wan N, Li S (2016). Land use regression

modeling of $PM_{2.5}$ concentrations at optimized spatial scales. Atmos, 8(1): 1

Zou B, Peng F, Wan N, Wilson J G, Xiong Y (2014). Sulfur dioxide exposure and environmental justice: a multi-scale and source-specific perspective. Atmos Pollut Res, 5(3): 491–499

Zou B, Pu Q, Bilal M, Weng Q, Zhai L, Nichol J E (2016a). High-resolution satellite mapping of fine particulates based on geographically weighted regression. IEEE Geosci Remote Sens Lett, 13(4): 495–499

Zou B, Xu S, Sternberg T, Fang X (2016b). Effect of land use and cover change on air quality in urban sprawl. Sustainability, 8(7): 677

Zou B, You J, Lin Y, Duan X, Zhao X, Xin F, Campen M J, Li S (2019). Air pollution intervention and life-saving effect in China. Environ Int, doi: 10.1016/j.envint.2018.10.045